Dyes and Pigments 134 (2016) 427–433

Contents lists available at ScienceDirect

Dyes and Pigments

journal homepage: www.elsevier.com/locate/dyepig

Chiral benzo-fused Aza-BODIPYs with optical activity extending into the NIR range

Lu Zhang, Luyang Zhao, Kang Wang, Jianzhuang Jiang*

Beijing Key Laboratory for Science and Application of Functional Molecular and Crystalline Materials, Department of Chemistry, University of Science and Technology Beijing, Beijing 100083, China

ARTICLE INFO

Article history:
Received 29 June 2016
Received in revised form
26 July 2016
Accepted 30 July 2016
Available online 1 August 2016

Keywords:
Chirality
Aza-BODIPY
Near-infrared spectroscopy

ABSTRACT

Chiral benzo-fused aza-BODIPYs, namely *N*,*N*-difluoroboryl-[(dinaphtho[1,2-*e*:1′,2′-*g*]-1,4-dioxocine)-1-[*N*-(3-phenyl-2H-isoindole-1-yl)methylene]-3-phenyl-1H-isoindol-1-ylidene)amine] (**1**) and *N*,*N*-difluoroboryl-[(dinaphtho[1,2-*e*:1′,2′-*g*]-1,4-dioxocine)-1-[(dinaphtho[1,2-*e*:1′,2′-*g*]-1,4-dioxocine)-*N*-(3-phenyl-2H-isoindole-1-yl)methylene]-3-phenyl-1H-isoindol-1-ylidene)amine] (**2**), have been synthesized and spectroscopically characterized. Fusion of benzene moieties onto the BODIPY periphery in combination with the introduction of peripheral chiral binaphthyl substituents renders the extension of optical activity of resulting chiral benzo-fused aza-BODIPYs into the near-IR (NIR) range, representing the first chiral BODIPYs with NIR optically activity. For comparative study, *N*,*N*-difluoroboryl-[*N*-(3-phenyl-2H-isoindol-1-yl)-*N*-(3-phenyl-1H-isoindol-1-ylidene)amine] (**0**) was also prepared and characterized in a similar manner.

1. Introduction

Boron dipyrromethenes (BODIPYs) are a special class of dipyrrolic conjugated molecular systems that have been widely studied and applied in the field of biochemical labeling, fluorescent sensors, and sensitizers for solar cells and laser dyes owning to their fascinating physicochemical properties such as high fluorescence quantum yields, narrow absorption and emission bands with high intensities, reasonably long excited singlet state lifetime, and good solubility and stability in common organic solvent systems [1,2]. The absorption and emission properties of BODIPYs can be easily tuned through chemical modifications over the meso-carbon atom, fluoride atoms of the BF_2-group, and BODIPY periphery and core [3]. Actually, replacement of the meso-carbon atom in the general BODIPY dyes by nitrogen atom in combination with the fusion of benzene moiety onto the pyrrole moieties of BODIPY chromophore results in the benzo-fused aza-BODIPY compounds with extended π-system and appearance of the electronic absorption and emission bands in the near-infrared (NIR) range [3b,4]. This in turn endows such kind of benzo-fused aza-BODIPY dyes great application potentials in fiber optic telecommunication, optical imaging, and in particular the cellular and *in vivo* biological studies due to the minimum photo-damage to biological samples and minimum interference from background auto-fluorescence by biomolecules in the living systems [5].

On the other hand, chirality has been one of the most fascinating features commonly found in nature [6]. Due to the relatively easy investigation by means of optical techniques, various chiral dyes including chiral porphyrins and phthalocyanines/subphthalocyanines have been designed and studied [7]. This is surely true for the chiral BODIPY derivatives with the optical activity limited in the UV–visible range [8]. However, chiral BODIPY derivatives with the optical activity extending into the NIR region still remain unreported thus far, to the best of our knowledge.

In this paper, chiral benzo-fused aza-BODIPYs, namely *N*,*N*-difluoroboryl-[(dinaphtho[1,2-*e*:1′,2′-*g*]-1,4-dioxocine)-1-[*N*-(3-phenyl-2H-isoindole-1-yl)methylene]-3-phenyl-1H-isoindol-1-ylidene)amine] (**1**) and *N*,*N*-difluoroboryl-[(dinaphtho[1,2-*e*:1′,2′-*g*]-1,4-dioxocine)-1-[(dinaphtho[1,2-*e*:1′,2′-*g*]-1,4-dioxocine)-*N*-(3-phenyl-2H-isoindole-1-yl)methylene]-3-phenyl-1H-isoindol-1-ylidene)amine] (**2**), have been synthesized and spectroscopically characterized. Fusion of benzene moieties onto the BODIPY periphery in combination with the introduction of peripheral chiral binaphthyl substituents renders the extension of optical activity of resulting chiral benzo-fused aza-BODIPYs into the near-IR (NIR) range, representing the first chiral BODIPYs with

* Corresponding author.
E-mail address: jianzhuang@ustb.edu.cn (J. Jiang).

http://dx.doi.org/10.1016/j.dyepig.2016.07.039
0143-7208/

NIR optically activity. For comparative study, *N*,*N*-difluoroboryl-[*N*-(3-phenyl-2H-isoindol-1-yl)-*N*-(3-phenyl-1H-isoindol-1-ylidene)amine] (**0**) was also prepared and characterized in a similar manner.

2. Experimental section

2.1. General remarks

Column chromatography was carried out on silica gel (Merck, Kieselgel 60, 70–230 mesh) with the indicated eluents. CH_2Cl_2 was freshly distilled with CaH_2 under nitrogen atmosphere. All other reagents and solvents were used as received. The compounds (*R*)/(*S*)-benzo[*b*]dinaphtho[2,1-*e*:1′,2′-*g*] [1,4]dioxocine-2,3- dicarbonitrile were prepared according to the literature procedure [9].

The ^{1}H NMR spectra and ^{1}H-^{1}H COSY spectra were recorded on a Bruker DPX 400 spectrometer in $CDCl_3$ with shifts referenced to $SiMe_4$ (0.00 ppm). Electronic absorption spectra were recorded on a Hitachi U-4100 spectrophotometer. MALDI-TOF mass spectra were taken on a Bruker BIFLEX III ultra-high resolution Fourier transform ion cyclotron resonance (FT-IR) mass spectrometer with alpha-cyano-4-hydroxy cinnamic acid as the matrix. Elemental analyses were performed on an Elementar Vavio El III elemental analyzer. Steady-state fluorescence spectroscopic studies and absolute fluorescent quantum yields were performed on an Edinburgh Instruments FLS920 fluorescence spectrometer with the excitation at 650 nm. Time-resolved fluorescence lifetime experiments were performed by the time-correlated single-photon-counting (TCSPC) technique on an Edinburgh Instruments FLS900 fluorescence spectrometer. Electrochemical measurements were carried out with a BAS CV-50W voltammetric analyzer. The reference electrode was Ag^+/Ag (a solution of 0.01 M $AgNO_3$ and 0.1 M TBAP in acetonitrile), which was connected to the solution by a Luggin capillary whose tip was placed close to the working electrode. It was corrected for junction potentials by being referenced internally to the ferrocenium/ferrocene (Fc^+/Fc) couple [$E_{1/2}$(Fc^+/Fc) = 0.501 V *vs.* SCE].

2.2. Synthesis of (R)/(S)-*1a*

Phenyl magnesium bromide (3.0 mol/L in diethyl ether, 1 mL) was added to a suspension of (*R*)/(*S*)-benzo[*b*]dinaphtho[2,1-*e*:1′,2′-*g*] [1,4]dioxocine-2,3-dicarbonitrile (410 mg, 1 mmol) and 1,2-Dicyanobenzene (128 mg, 1 mmol) in anhydrous diethyl ether (10 mL) at 0 °C under nitrogen. The reaction mixture was allowed to warm to room temperature and stirred for additional 3 h. Then the reaction mixture was evaporated to dryness and formamide (30 mL) was added to the reaction system under nitrogen. The reaction mixture was further heated at 150 °C for 30 min. After being cooled to room temperature, the mixture was diluted with dichloromethane and washed with water and saturated NaCl (aq.). Upon drying over anhydrous Na_2SO_4, the organic layer was condensed in vacuo and the crude product was purified by column chromatography over silica gel using CH_2Cl_2/petroleum ether (1:1) as the eluent to give a blue band, which was further purified using gel chromatography with CH_2Cl_2 as eluent to give the first blue band as compound **2a**, then the second blue band as compound **1a**, following by the third blue band as compound **0a**. The following recrystallization from CH_2Cl_2 and MeOH gave **0a** as dark blue powder (23.1 mg, 3.4%), **1a** as dark blue powder (21.0 mg, 3.1%), **2a** as dark blue powder (9.5 mg, 1.4%). **1a**:^{1}H NMR (400 MHz, $(CD_3)_2SO$): δ 7.43–7.52 (m, 12H, binaphthyl-H, para-H, *β*-benzo-H), 7.56–7.60 (m, 5H, meta-H, *β*-benzo-H), 7.65–7.69 (m, 4H, *α*-benzo-H, binaphthyl-H), 7.80 (d, 2H, *J* = 8.0 Hz, binaphthyl-H), 7.86 (d, 2H, *J* = 8.0 Hz, binaphthyl-H), 8.10–8.12 (m, 4H, ortho-H), 8.17–8.20 (m, 8H, *α*-benzo-H, binaphthyl-H). MALDI-TOF MS: an isotopic cluster peaking at *m*/*z* 679.40; Calculated for $C_{48}H_{29}N_3O_2$, 679.23. Anal. Calcd (%) for $C_{48}H_{29}N_3O_2 \cdot CH_3OH$: C, 82.68; H, 4.67; N, 5.90; Found: C, 82.51; H, 4.99; N, 5.80.

2.3. Synthesis of (R)/(S)-*1*

Compound (*R*)/(*S*)-**1a** (68 mg, 0.1 mmol) was dissolved in dichloroethane (2 mL), then diisopropylethylamine (88 μL, 0.5 mmol) was added. The mixture was stirred for 1 h and $BF_3 \cdot OEt_2$ (63 μL, 0.5 mmol) was added at room temperature. This mixture was stirred at room temperature until complete conversion of the starting material after *ca.* 5 h as monitored by thin layer chromatography (TLC). The reaction mixture was then quenched with water and extracted twice with dichloromethane (100 mL). Upon drying over anhydrous Na_2SO_4, the organic layer was condensed in vacuo and the crude product was purified by column chromatography over silica gel using CH_2Cl_2/petroleum ether (1:1) as the eluent to give a green band. Recrystallization from CH_2Cl_2 and MeOH provided a green solid with the yield of 51.6 mg (71%). ^{1}H NMR (400 MHz, $(CD_3)_2SO$): δ 7.42–7.48 (m, 6H, *β*-benzo-H, *α*-benzo-H, binaphthyl-H), 7.54–7.59 (m, 7H, binaphthyl-H, meta-H, para-H), 7.62–7.64 (m, 2H, *α*-benzo-H, binaphthyl-H), 7.67 (d, 1H, *J* = 8.0 Hz, binaphthyl-H), 7.69 (d, 1H, *J* = 8.0 Hz, binaphthyl-H), 7.72 (d, 1H, *J* = 8.0 Hz, binaphthyl-H), 7.88 (m, 4H, ortho-H), 8.00 (s, 1H, *α*-benzo-H), 8.06–8.08 (m, 2H, *α*-benzo-H, binaphthyl-H), 8.10 (d, 1H, *J* = 8.0 Hz, binaphthyl-H), 8.12 (d, 1H, *J* = 8.0 Hz, binaphthyl-H), 8.15 (d, 1H, *J* = 8.0 Hz, binaphthyl-H). MALDI-TOF MS: an isotopic cluster peaking at *m*/*z* 727.45; Calculated for $C_{48}H_{28}BF_2N_3O_2$, 727.22. Anal. Calcd (%) for $C_{48}H_{28}BF_2N_3O_2 \cdot 0.5CH_2Cl_2$: C, 75.65; H, 3.80; N, 5.46; Found: C, 75.99; H, 4.01; N, 5.78.

2.4. Synthesis of (R)/(S)-*2a*

By employing the above-described procedure for Synthesis of (*R*)/(*S*)-**1a** with (*R*)/(*S*)-benzo[*b*]dinaphtho[2,1-*e*:1′,2′-*g*] [1,4]dioxocine-2,3-dicarbonitrile (410 mg, 1 mmol) instead of (*R*)/(*S*)-benzo[*b*]dinaphtho[2,1-*e*:1′,2′-*g*] [1,4]dioxocine-2,3-dicarbonitrile (410 mg, 1 mmol) and 1,2-Dicyanobenzene (128 mg, 1 mmol) as starting material, compound **2a** was obtained as a blue solid with the yield of 21.6 mg (4.5%). ^{1}H NMR (400 MHz, $(CD_3)_2SO$): δ 7.48–7.53 (m, 10H, binaphthyl-H, para-H), 7.61–7.63 (m, 6H, meta-H, *α*-benzo-H), 7.69–7.73 (m, 4H, binaphthyl-H), 7.85 (d, 2H, *J* = 8.0 Hz, binaphthyl-H), 7.90 (d, 2H, *J* = 8.0 Hz, binaphthyl-H), 8.15–8.17 (m, 6H, *α*-benzo-H, ortho-H), 8.20–8.25 (m, 8H, binaphthyl-H). MALDI-TOF MS: an isotopic cluster peaking at *m*/*z* 961.62; Calculated for $C_{68}H_{39}N_3O_4$, 961.29. Anal. Calcd (%) for $C_{68}H_{39}N_3O_4 \cdot 2CH_3OH$: C, 81.93; H, 4.62; N, 4.09; Found: C, 81.59; H, 4.97; N, 3.95.

2.5. Synthesis of (R)/(S)-*2*

By employing the above-described procedure for the synthesis of (*R*)/(*S*)-**1** with compound (*R*)/(*S*)-**2a** (96 mg, 0.1 mmol) instead of (*R*)/(*S*)-**1a** (68 mg, 0.1 mmol) as starting material, compound **2** was obtained as green solid with the yield of 67.6 mg (67%). ^{1}H NMR (400 MHz, $(CD_3)_2SO$:$CDCl_3$ = 3:1): δ 7.38–7.41 (m, 4H, binaphthyl-H), 7.45 (m, 4H, binaphthyl-H, *α*-benzo-H), 7.48–7.54 (m, 4H, binaphthyl-H), 7.57–7.58 (m, 8H, binaphthyl-H, meta-H, para-H), 7.62 (d, 2H, *J* = 8.0 Hz, binaphthyl-H), 7.67 (d, 2H, *J* = 8.0 Hz, binaphthyl-H), 7.87 (d, 2H, *J* = 8.0 Hz, ortho-H), 7.92 (s, 2H, *α*-benzo-H), 8.00 (d, 2H, *J* = 8.0 Hz, binaphthyl-H), 8.04–8.07 (m, 4H, binaphthyl-H), 8.10 (d, 2H, *J* = 8.0 Hz, binaphthyl-H). MALDI-TOF MS: an isotopic cluster peaking at *m*/*z* 1009.65; Calculated for $C_{68}H_{38}BF_2N_3O_4$, 1009.29. Anal. Calcd (%) for

$C_{68}H_{38}BF_2N_3O_4 \cdot 0.5CH_2Cl_2$: C, 78.18; H, 3.74; N, 3.99; Found: C, 78.42; H, 3.95; N, 3.79.

3. Results and discussion

3.1. Design and synthesis

(*R*)/(*S*)-Benzo[*b*]dinaphtho[2,1-*e*:1′,2′-*g*] [1,4]dioxocine-2,3-dicarbonitrile were prepared following published procedure [9]. Reaction of this precursor with 1,2-dicyanobenzene in the presence of phenyl magnesium bromide in formamide at 150 °C resulted in a mixture of *N*-(3-phenyl-2H-isoindol-1-yl)-*N*-(3-phenyl-1H-isoindol-1-ylidene)amine (**0a**), (dinaphtho[1,2-*e*:1′,2′-*g*]-1,4-dioxocine)-1-[*N*-(3-phenyl-2H-isoindole-1-yl)methylene]-3-phenyl-1H-isoindol-1-ylidene)amine (**1a**), and (dinaphtho[1,2-*e*:1′,2′-*g*]-1,4-dioxocine)-1-[(dinaphtho[1,2-*e*:1′,2′-*g*]-1,4-dioxocine)-*N*-(3-phenyl-2H-isoindole-1-yl)methylene]-3-phenyl-1H-isoindol-1-ylidene)amine (**2a**), Scheme S1 (Supporting Information). Gel chromatography with CH_2Cl_2 as eluent afforded pure **0a**, **1a**, and **2a** in the yield of 3.4, 3.1, and 1.4%, respectively. Treatment of which with diisopropylethylamine and $BF_3 \cdot OEt_2$ gave corresponding benzo-fused 3,5-diaryl aza-BODIPY compounds including *N*,*N*-difluoroboryl-[*N*-(3-phenyl-2H-isoindol-1-yl)-*N*-(3-phenyl-1H-isoindol-1-ylidene)amine] (**0**), *N*,*N*-difluoroboryl-[(dinaphtho[1,2-*e*:1′,2′-*g*]-1,4-dioxocine)-1-[*N*-(3-phenyl-2H-isoindole-1-yl)methylene]-3-phenyl-1H-isoindol-1-ylidene)amine] (**1**), and *N*,*N*-difluoroboryl-[(dinaphtho[1,2-*e*:1′,2′-*g*]-1,4-dioxocine)-1-[(dinaphtho[1,2-*e*:1′,2′-*g*]-1,4-dioxocine)-*N*-(3-phenyl-2H-isoindole-1-yl)methylene]-3-phenyl-1H-isoindol-1-ylidene)amine] (**2**) in the yield of 70, 71, and 67%, Scheme 1. Both **1** and **2** were characterized by ^{1}H NMR, ^{1}H-^{1}H COSY, and mass spectroscopies in addition to elemental analysis, Figs. S1-S6 and Tables S1 and S2 (Supporting Information). At the end of this section, it is worth noting that for the ease of isolation both the symmetrical benzo-fused aza-BODIPY precursors (**0a**, **2a**) and derivatives (**0**, **2**) could actually be easily prepared with 1,2-dicyanobenzene or (*R*)/(*S*)-benzo[*b*]dinaphtho[2,1-*e*:1′,2′-*g*] [1,4]dioxocine-2,3-dicarbonitrile instead of mixed 1,2-dicyanobenzene and (*R*)/(*S*)-benzo[*b*]dinaphtho[2,1-*e*:1′,2′-*g*] [1,4]dioxocine-2,3-dicarbonitrile as starting material following the same reaction procedure as detailed above.

3.2. Electronic absorption and circular dichroism (CD) spectroscopy

The electronic absorption spectra of **0**–**2** were recorded in CH_2Cl_2 and the data are summarized in Table S3 (Supporting Information). As shown in Fig. 1, Figs. S7, and S8 (Supporting Information), an intense $S_0 \rightarrow S_1$ band appears at 712 nm for the reference benzo-fused 3,5-diaryl aza-BODIPY compound **0** with a shoulder band appearing at 655 nm. In addition, this compound also exhibits a weak band at 309 nm due to the $S_0 \rightarrow S_2$ transition of the BODIPY system [10]. Along with the incorporation of one binaphthyl group onto the benzene moiety of the benzo-fused 3,5-diaryl aza-BODIPY skeleton, the $S_0 \rightarrow S_1$ band slightly red-shifts to 717 nm for **1** due to the somewhat p-π conjugation between the peripheral oxygen atoms and the central BODIPY chromophore [11]. As a consequence, further incorporation of the second binaphthyl group onto the remaining benzene ring in the molecule of **1** leads to further red-shift of the $S_0 \rightarrow S_1$ band to 722 nm for **2**.

The CD spectra of the chiral fluorophores **1** and **2** are also displayed in Fig. 1 and Fig. S7 (Supporting Information). As can be clearly seen, perfect mirror image CD spectra are observed in the entire absorption region for both **1** and **2**. The CD intensity for both **1** and **2** reaches up to 30×10^2 deg M^{-1} cm^{-1}, in line with that for traditional optical active BODIPY chromophores [12]. In detail, the CD signals of **1S** is negative in the whole electronic absorption region, with significant $S_0 \rightarrow S_1$ band at *ca.* 717 nm, and $S_0 \rightarrow S_2$ band at *ca.* 300 nm. In a similar manner, negative significant CD signals of **2S** are observed at *ca.* 721 nm and 302 nm, belonging to $S_0 \rightarrow S_1$ band and $S_0 \rightarrow S_2$ band, respectively. In contrast, CD signals of both **1R** and **2R** are positive in the whole region with significant peaks at 719 nm and 300 nm for **1R**, and 723 nm and 302 nm for **2R**. Similar to the reported binaphthyl-linked phthalocyanines and subphthalocyanine [13], these intense CD signals of both **1** and **2** are induced from the peripheral chiral binaphthyl units since the central BODIPY chromophore is achiral while the CD of binaphthyl units appears at wavelengths shorter than *ca.* 260 nm. Following the mechanism of induced optical activity, the experimental phenomenon that the CD intensity of $S_0 \rightarrow S_2$ band is much larger than that of the $S_0 \rightarrow S_1$ band could be well explained on the basis of the fact that the induced CD intensity is proportional to $1/(\nu_N^2 - \nu_{BODIPY}^2)$ [14], where ν_N and ν_{BODIPY} are the frequencies of the absorption of naphthalene and BODIPY, respectively. This is further supported by the nearly two times of CD signal intensity for **2** with two chiral binaphthyl groups in comparison with that for **1** with only one chiral binaphthyl unit, Fig. 1 and Fig. S7 (Supporting Information).

To quantitatively evaluate the chiral dissymmetry of **1** and **2**, the anisotropic factor *g* was calculated according to the equation: $g = \theta/(33 \cdot \varepsilon)$ [15]. The *g* factor values of **1** and **2** are summarized in Table S4 (Supporting Information). As can be found, the *g* factor of compound **1** is 1.4×10^{-4} for $S_0 \rightarrow S_1$ band and 12.8×10^{-4} for $S_0 \rightarrow S_2$ band, which amounts to 2.6×10^{-4} and 16.4×10^{-4}, respectively, for the $S_0 \rightarrow S_1$ and $S_0 \rightarrow S_2$ band of **2**, indicating the considerable chirality-induced ability of the binaphthyl unit. The *g* factor of **2** is larger than that of **1**, revealing the effect of the number of binaphthyl units and confirming the induced chirality nature for both **1** and **2**.

3.3. Electronic structures and theoretical investigation

In order to get further insight into electronic absorption and CD spectra of **1** and **2**, DFT and TD-DFT calculations were performed at M06/6-311G(d) level [16]. The optimized molecular structures

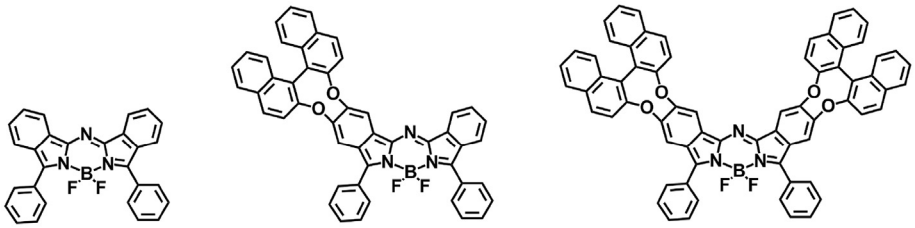

Scheme 1. Schematic molecular structures of benzo-fused aza-BODIPYs.

including both (*R*)- and (*S*)-enantiomers of both **1** and **2** are shown in Fig. 2 and Fig. S9 (Supporting Information). The frontier molecular orbital (MO) maps of **2S** are shown in Fig. 3 and that of **1S** in Fig. S10 (Supporting Information). The excited states under TD-DFT calculation and simulated absorption and CD spectra of **1** and **2** are shown at the bottom of Fig. 1 and Fig. S7 (Supporting Information). The electron transitions of significant excited states and corresponding oscillator strength (*f*) and rotational strength (*R*) are summarized in Table 1. As can be found, despite the slight overestimation of the vertical transition energies, the simulated electronic absorption spectra of **1** and **2** are in good agreement with the experimental results. The $S_0 \rightarrow S_1$ band absorptions are estimated at 618 nm for **2S**, 610 nm for **1S**, and 600 nm for **0**. The $S_0 \rightarrow S_1$ band for all the three compounds is mainly contributed by the electron transitions from HOMO→LUMO, which are located mainly on the benzo-fused aza-BODIPY chromophore [4c,5a]. The participation of peripheral oxygen atoms in the electron transitions seems to result in the redshift of **1** and **2** in comparison with that for **0** due to the conjugation between oxygen atoms and the central BODIPY chromophore according to the electron transition density

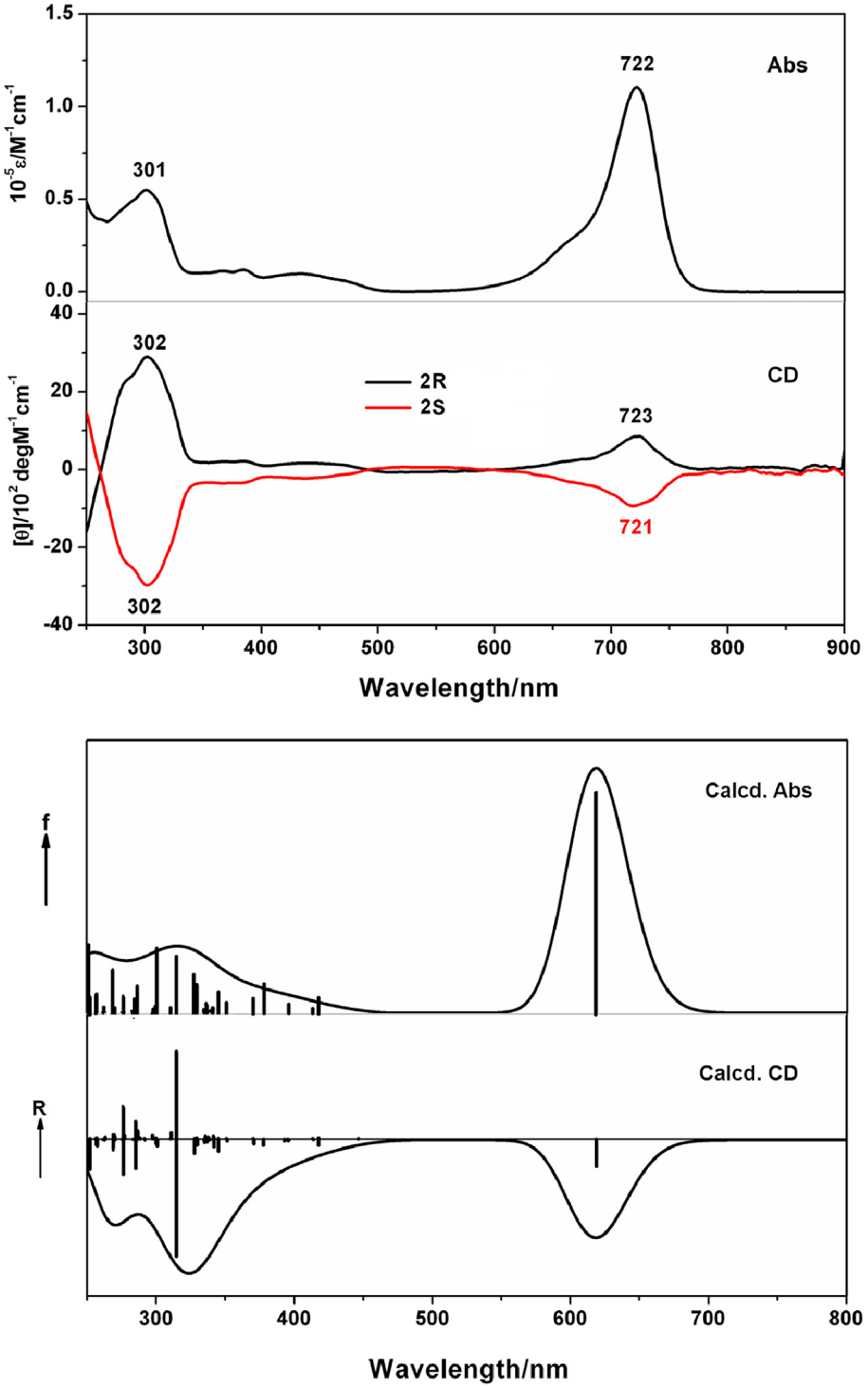

Fig. 1. Electronic absorption spectra and CD of **2** in CH_2Cl_2, and calculated absorption spectra and CD of **2S**.

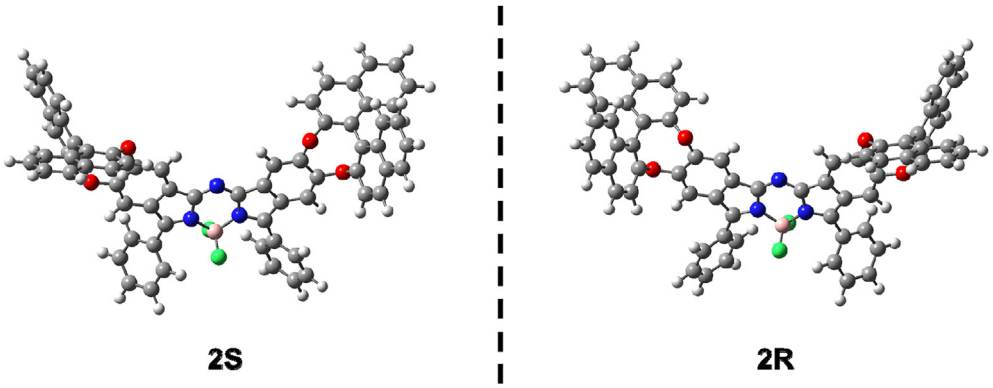

Fig. 2. Simulated molecular structures of **2S** and **2R**.

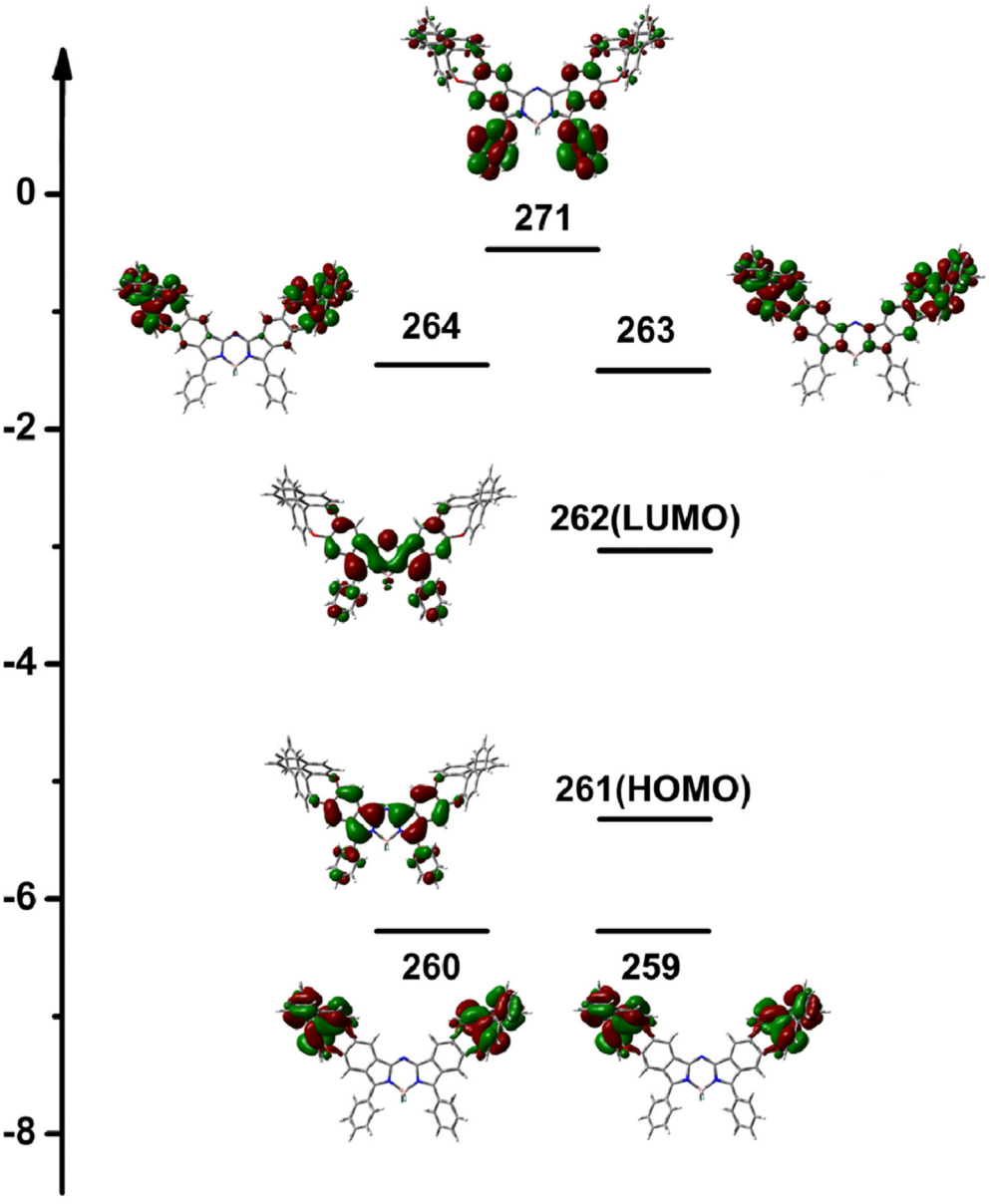

Fig. 3. Partial molecular energy diagram and orbitals of **2S**.

Table 1
The calculated excited wavelength (λ), oscillator strength (f), rotational strength (R), and electron transition compositions of important transitions for **0**, **1S** and **2S**.

Compound	λ (nm)	f	R (length)[a]	Transition composition[b]	
0	600	0.76	–	H→L[c]	98%
	298	0.21	–	H→L+3	92%
1	610	0.90	−36.34	H→L	98%
	315	0.15	−68.56	H−1→L+1	94%
	300	0.23	−32.56	H→L+6	77%
2	618	1.05	−127.20	H→L	98%
	315	0.27	−557.90	H−2→L+2	46%
				H−1→L+1	49%
	300	0.31	−34.77	H→L+9	85%
				H→L+12	7%

[a] The unit is 10^{-40} erg-esu-cm/Gauss.
[b] The transition compositions with more than 5% contribution are listed.
[c] H refers to HOMO, and L refers to LUMO.

difference plots, Table S5 (Supporting Information). This well reproduces the experimental result. The band observed at 301 nm by UV–vis spectroscopy can be represented by the calculated transitions at 315 nm and 300 nm with relatively large oscillator strengths. However, the transition at 315 nm is composed by HOMO−2→LUMO+2 and HOMO−1→LUMO+1 with electrons localizing mainly on the binaphthyl units, while the transition at 301 nm is composed by HOMO→LUMO+9, in which the electrons locate mainly on the central BODIPY chromophore. As a consequence, these two transitions exhibit essential different electronic transition nature despite their close energies. This is also true for **1**, Table S6 (Supporting Information). The simulated CD spectra of **1S** and **2S** also match well with the experimental ones in terms of both the sign and relative intensity.

3.4. Fluorescence spectra

The steady-state fluorescence spectra of **0**–**2** were measured in CH_2Cl_2 and toluene with corresponding data summarized in Table S8 (Supporting Information). As shown in Fig. S12 (Supporting Information), the fluorescence emission spectra of **0**–**2** in CH_2Cl_2 display mirror-symmetrical bands relative to the absorption spectra with almost the same Stokes shifts of *ca.* 590 cm^{-1}. The emission maxima of **0**–**2** appear at 744 nm, 749 nm, and 754 nm, respectively, showing red-shift in comparison with their absorption spectra. The fluorescence quantum yields (Φ) of **0**–**2** are 12.35%, 11.30%, and 7.77%, respectively, and their fluorescence lifetime (τ_F) are 2.0 ns, 1.9 ns, and 1.8 ns? The decrease in both the quantum yields and lifetime along with the increase in the number of the binaphthyl unit incorporated actually results from the increased vibrational modes along with the increase in the molecular size in the same order, which in turn lead to more non-radiative decay. The emission spectra of **0**–**2** in toluene are similar to those in CH_2Cl_2 despite slightly further red-shift of *ca.* 3 nm in the emission maxima in comparison with that in CH_2Cl_2. Meanwhile, the fluorescence emission intensity and lifetime in toluene get a bit of larger than those in CH_2Cl_2 due to the decrease of the solvent polarity, Table S8 (Supporting Information).

3.5. Electrochemistry

The redox behavior of **0**–**2** was studied by cyclic voltammetry (CV) in CH_2Cl_2. The half-wave redox potentials are shown in Fig. S13 and summarized in Table S9 (Supporting Information). Within the electrochemical window of CH_2Cl_2, the reference compound **0** displays two quasi-reversible one-electron oxidations at +1.38 and + 0.97 V and one quasi-reversible one-electron reduction at −0.61 V. The potential difference between the first oxidation and the first reduction, which reflects the HOMO-LUMO gap, was found to be 1.58 V for **0**. This is also true for the counterparts **1** and **2** with two quasi-reversible one-electron oxidations at +1.39 and + 0.97 V and one quasi-reversible one-electron reduction at −0.58 V for **1** and two quasi-reversible one-electron oxidations at +1.41 and + 0.96 V and one quasi-reversible one-electron reduction at −0.56 V for **2**. Interestingly, along with the increase in the number of binaphthyl group incorporated onto the benzo-fused aza-BODIPY skeleton, the potential difference between the first oxidation and the first reduction gets decreased from 1.58 V for **0** to 1.55 V for **1** and 1.52 V for **2** due to the p-π conjugation between the peripheral oxygen atoms and the BODIPY chromophore. This result is in line with the red-shift of the lowest energy absorption band of these compounds in the same order.

4. Conclusion

In conclusion, chiral benzo-fused aza-BODIPYs with optical activity extending into the NIR range have been synthesized and spectroscopically characterized for the first time. This will arouse a wide range of interest in the design and synthesis of novel chiral benzo-fused aza-BODIPY compounds due not only to their intrinsic scientific importance but also their potential applications in biological measurements and cellular imaging.

Acknowledgement

Financial support from the National Key Basic Research Program of China (No. 2013CB933402), the National Natural Science Foundation of China (No. 21290174 and 21301017), Beijing Municipal Commission of Education, and University of Science and Technology Beijing is gratefully acknowledged.

Appendix A. Supplementary data

Supplementary data related to this article can be found at http://dx.doi.org/10.1016/j.dyepig.2016.07.039.

References

[1] (a) Treibs A, Kreuzer FH. Difluoroboryl complexes of di- and tripyrrylmethenes. Liebigs Ann Chem 1968;718:208–23.
(b) Boens N, Leen V, Dehaen W. Fluorescent indicators based on BODIPY. Chem Soc Rev 2012;41:1130–72.
(c) Wu Y, Mao X, Ma X, Huang X, Cheng Y, Zhu C. Synthesis and fluorescence properties of chiral near-infrared emissive polymers incorporating BODIPY derivatives and (S)-binaphthyl. Macromol Chem Phys 2012;213:2238–45.
(d) Ulrich G, Ziessel R, Harriman A. The chemistry of fluorescent Bodipy dyes: versatility unsurpassed. Angew Chem Int Ed 2008;47:1184–201.
(e) Feng J, Liang B, Wang D, Xue L, Li X. Novel fluorescent dyes with fused perylene tetracarboxylic diimide and BODIPY analogue structures. Org Lett 2008;10:4437–40.
(f) Wising U, Berntsson T, Asblad A. Energy system consequences when installing an advanced delignification process. Can J Chem Eng 2006;84:108–15.
(g) Chen Y, Wang H, Wan L, Bian Y, Jiang J. 8-hydroxyquinoline-substituted boron-dipyrromethene compounds: synthesis, structure, and OFF-ON-OFF type of pH-sensing properties. J Org Chem 2011;76:3774–81.
(h) Chen Y, Wan L, Yu X, Li W, Bian Y, Jiang J. Rational design and synthesis for versatile FRET ratiometric sensor for Hg^{2+} and Fe^{2+}: a flexible 8-hydroxyquinoline benzoate linked bodipy-porphyrin dyad. Org Lett 2011;13:5774–7.
(i) Chen Y, Qi D, Zhao L, Cao W, Huang C, Jiang J. Boron-phenylpyrrin dyes: facile synthesis, structure, and pH-sensitive properties. Chem Eur J 2013;19:7342–7.
(j) Zhang L, Chen Y, Jiang J. Solid state fluorescent functionalized-triphenylamine Bodipy detector for HCl vapor with high stability and absolute fluorescent quantum yield. Dyes Pigm 2016;124:110–9.
[2] (a) Karolin J, Johansson LBA, Strandberg L, Ny T. Fluorescence and absorption spectroscopic properties of dipyrromethene boron difluoride (BODIPY) derivatives in liquids, lipid membranes, and proteins. J Am Chem Soc 1994;116:

7801–6.
(b) Merino EJ, Weeks KM. Facile Conversion of aptamers into sensors using a 2′-ribose-linked fluorophore. J Am Chem Soc 2005;127:12766–7.
(c) Domaille DW, Zeng L, Chang CJ. Visualizing ascorbate-triggered release of labile copper within living cells using a ratiometric fluorescent sensor. J Am Chem Soc 2010;132:1194–5.
(d) Rurack K, Kollmannsberger M, Daub J. Molecular switching in the near infrared (NIR) with a functionalized boron-dipyrromethene dye. Angew Chem Int Ed 2001;40:385–7.
(e) Rurack K, Kollmannsberger M, Resch-Genger U, Daub J. A selective and sensitive fluoroionophore for Hg^{II}, Ag^{I}, and Cu^{II} with virtually decoupled fluorophore and receptor units. J Am Chem Soc 2000;122:968–9.
(f) Gabe Y, Urano Y, Kikuchi K, Kojima H, Nagano T. Highly sensitive fluorescence probes for nitric oxide based on boron dipyrromethene chromophore-rational design of potentially useful bioimaging fluorescence probe. J Am Chem Soc 2004;126:3357–67.
(g) Arbeloa TL, Arbeloa FL, Arbeloa IL, Garcia-Moreno I, Costela A, Sastre R, et al. Correlations between photophysics and lasing properties of dipyrromethene-BF_2 dyes in solution. Chem Phys Lett 1999;299:315–21.
[3] (a) Lu H, Mack J, Yang Y, Shen Z. Structural modification strategies for the rational design of red/NIR region BODIPYs. Chem Soc Rev 2014;43:4778–823.
(b) Chen GR, Fei ZB, Huang XT, Xie YY, Xu JL, Gola J, et al. Ring-closing olefin metathesis of 3,3′-(D-glycopyranosylidene)bis(1-propene) compounds as a route to anomeric spiro sugars. Eur J Org Chem 2001:2939–46.
(c) Loudet A, Burgess K. BODIPY dyes and their derivatives: syntheses and spectroscopic properties. Chem Rev 2007;107:4891–932.
[4] (a) Shimizu S, Murayama A, Haruyama T, Iino T, Mori S, Furuta H, et al. Benzo[c,d]indole-containing aza-BODIPY dyes: asymmetrization-induced solid-state emission and aggregation-induced emission enhancement as new properties of a well-known chromophore. Chem Eur J 2015;21:12996–3003.
(b) Descalzo AB, Xu HJ, Xue ZL, Hoffmann K, Shen Z, Weller MG, et al. Phenanthrene-fused boron-dipyrromethenes as bright long-wavelength fluorophores. Org Lett 2008;10:1581–4.
(c) Donyagina VF, Shimizu S, Kobayashi N, Lukyanets EA. Synthesis of N,N-difluoroboryl complexes of 3,3′-diarylazadiisoindolylmethenes. Tetrahedron Lett 2008;49:6152–4.
(d) Kubo Y, Minowa Y, Shoda T, Takeshita K. Synthesis of a new type of dibenzopyrromethene-boron complex with near-infrared absorption property. Tetrahedron Lett 2010;51:1600–2.
(e) Bandi V, Gobeze HB, D'Souza F. Ultrafast photoinduced electron transfer and charge stabilization in donor-acceptor dyads capable of harvesting near-infrared light. Chem Eur J 2015;21:11483–94.
(f) Majumdar P, Mack J, Nyokong T. Synthesis, characterization and photophysical properties of an acenaphthalene fused-ring-expanded NIR absorbing aza-BODIPY dye. RSC Adv 2015;5:78253–8.
[5] (a) Lu H, Shimizu S, Mack J, Shen Z, Kobayashi N. Synthesis and spectroscopic properties of fused-ring-expanded aza-boradiazaindacenes. Chem Asian J 2011;6:1026–37.
(b) Yuan L, Lin W, Zheng K, He L, Huang W. Far-red to near infrared analyte-responsive fluorescent probes based on organic fluorophore platforms for fluorescence imaging. Chem Soc Rev 2013;42:622–61.
(c) Jiang XD, Xi D, Sun C, Guan J, He M, Xiao LJ. Synthesis of a pyrene-fused aza-BODIPY as a near-infrared dye having the absorption maximum at 746 nm. Tetrahedron Lett 2015;56:4868–70.
(d) Wu D, Cheung S, Devocelle M, Zhang LJ, Chen ZL, O'Shea DF. Synthesis and assessment of a maleimide functionalized BF_2 azadipyrromethene near-infrared fluorochrome. Chem Commun 2015;51:16667–70.
(e) Weissleder R, Pittet MJ. Imaging in the era of molecular oncology. Nature 2008;452:580–9.
(f) Wu W, Yao L, Yang T, Yin R, Li F, Yu Y. NIR-light-induced deformation of cross-linked liquid-crystal polymers using upconversion nanophosphors. J Am Chem Soc 2011;133:15810–3.
(g) Jing X, Yu F, Chen L. Visualization of nitroxyl (HNO) in vivo via a lysosome-targetable near-infrared fluorescent probe. Chem Commun 2014;50(91):14253–6.
(h) Liu P, Jing X, Yu F, Lv C, Chen L. A near-infrared fluorescent probe for the selective detection of HNO in living cells and in vivo. Analyst 2015;140(13):4576–83.
[6] (a) Garoff RA, Litzinger EA, Connor RE, Fishman I, Armitage BA. Helical Aggregation of Cyanine Dyes on DNA Templates: effect of dye structure on formation of homo- and heteroaggregates. Langmuir 2002;18:6330–7.
(b) Wang M, Silva GL, Armitage BA. DNA-templated formation of a helical cyanine Dye J-aggregate. J Am Chem Soc 2000;122:9977–86.
(c) Pasternack RF, Giannetto A, Pagano P, Gibbs EJ. Self-assembly of porphyrins on nucleic acids and polypeptides. J Am Chem Soc 1991;113:7799–800.
(d) Green MM, Cheon KS, Yang SY, Park JW, Swansburg S, Liu W. Chiral studies across the spectrum of polymer science. Acc Chem Res 2001;34:672–80.
(e) Cornelissen JJLM, Donners JJJM, de Gelder R, Graswinckel WS, Metselaar GA, Rowan AE, et al. β-Helical polymers from isocyanopeptides. Science 2001;293:676–80.
(f) Cornelissen JJ, Rowan AE, Nolte RJ, Sommerdijk NA. Chiral architectures from macromolecular building blocks. Chem Rev 2001;101:4039–70.
(g) Alnoman RB, Rihn S, O'Connor DC, Black FA, Costello B, Waddell PG, et al. Circularly polarized luminescence from helically chiral N, N,O,O-boron-chelated dipyrromethenes. Chem Eur J 2016;22(1):93–6.
(h) Wu Y, Wang S, Li Z, Shen Z, Lu H. Chiral binaphthyl-linked BODIPY analogues: synthesis and spectroscopic properties. J Mater Chem C 2016;4(21):4668–74.
[7] (a) Lu J, Wu L, Jing L, Xu X, Zhang X. Synthesis, circular dichroism, and third-order nonlinear optical properties of optically active porphyrin derivatives bearing four chiral citronellal moieties. Dyes Pigm 2012;94:169–74.
(b) Lu J, Deng Y, Zhang X, Kobayashi N, Jiang J. Optically active mixed (Phthalocyaninato)(Porphyrinato) rare earth triple-decker complexes. Synthesis, spectroscopy, and effective chiral information transfer. Inorg Chem 2011;50:2562–7.
(c) Yang L, Zhou Y, Zhu M, Zhao L, Wei L, Bian Y. Stereochemistry and solid-state structure of an intrinsically chiral meso-patterned porphyrin: case study by NMR and single-crystal x-ray diffraction analysis. J Org Chem 2013;78:9949–55.
(d) Zhou Y, Zhang Y, Wang H, Jiang J, Bian Y, Muranaka A, et al. Mixed (Phthalocyaninato)(Porphyrinato) rare earth double-decker complexes with C_4 chirality: synthesis, resolution, and absolute configuration assignment. Inorg Chem 2009;48:8925–33.
(e) Zhou H, Wang K, Qi D, Jiang J. Chiral bis(phthalocyaninato) yttrium double-decker complexes. Synthesis, structure, spectroscopy, and electrochemistry. Dalton Trans 2014;43:1699–705.
(f) Wang K, Qi D, Wang H, Cao W, Li W, Jiang J. A chiral phthalocyanine dimer with well-defined supramolecular symmetry based on π-π interactions. Chem Eur J 2012;18:15948–52.
(g) Wang K, Zeng S, Wang H, Dou J, Jiang J. Magneto-chiral dichroism in chiral mixed (phthalocyaninato)(porphyrinato) rare earth triple-decker SMMs. Inorg Chem Front 2014;1:167–71.
(h) Zhao L, Wang K, Shang H, Jiang J. Novel chiral ABBB-type unsymmetrical phthalocyanine. Ring-expansion synthesis, spectroscopic, and electrochemical properties. Dyes Pigm 2015;120:52–6.
(i) Shang H, Zhao L, Qi D, Chen C, Jiang J. The First Five-membered-heterocycle-fused subphthalocyanine analogues: chiral tri(benzo[*b*]thiopheno)subporphyrazines. Chem Eur J 2014;20:16266–72.
[8] (a) Lu H, Mack J, Nyokong T, Kobayashi N, Shen Z. Optically active BODIPYs. Coord Chem Rev 2016;318:1–15.
(b) Beer G, Niederalt C, Grimme S, Daub J. Redox switches with chiroptical signal expression based on binaphthyl boron dipyrromethene conjugates. Angew Chem Int Ed 2000;39:3252–5.
(c) Beer G, Daub J, Rurack K. Chiral discrimination with a fluorescent boron-dipyrromethene dye. Chem Commun 2001;12:1138–9.
(d) Sanchez-Carnerero EM, Moreno F, Maroto BL, Agarrabeitia AR, Ortiz MJ, Vo BG, et al. Circularly polarized luminescence by visible-light absorption in a chiral *o*-BODIPY dye: unprecedented design of CPL organic molecules from achiral chromophores. J Am Chem Soc 2014;136:3346–9.
[9] Wang K, Wang H, Mack J, Li W, Kobayashi N, Jiang J. Chiral phthalocyanine with unambiguous absolute molecular structures for both enantiomers. Acta Chim Sin 2012;70:1791–7.
[10] (a) Zou B, Liu H, Mack J, Wang S, Tian J, Lu H, et al. A new aza-BODIPY based NIR region colorimetric and fluorescent chemodosimeter for fluoride. RSC Adv 2014;4:53864–9.
(b) Lu H, Mack J, Yang Y, Shen Z. Structural modification strategies for the rational design of red/NIR region BODIPYs. Chem Soc Rev 2014;43(13):4778–823.
(c) Harriman A, Izzet G, Ziessel R. Rapid energy transfer in cascade-type Bodipy dyes. J Am Chem Soc 2006;128(33):10868–75.
(d) Zhao Y, Lv X, Liu Y, Liu J, Zhang Y, Shi H, et al. The emission enhancement of the NIR distyryl Bodipy dyes by the indirect S0→S2 excitation and their application towards a Hg^{2+} probe. J Mater Chem 2012;22(23):11475–8.
[11] Chen Y, Cao W, Wang C, Qi D, Wang K, Jiang J. Four Dibutylamino substituents are better than eight in modulating the electronic structure and third-order nonlinear-optical properties of phthalocyanines. Inorg Chem 2016;55:3151–60.
[12] (a) Kolemen S, Cakmak Y, Kostereli Z, Akkaya EU. Atropisomeric dyes: axial chirality in orthogonal BODIPY oligomers. Org Lett 2014;16:660–3.
(b) Gossauer A, Nydegger F, Kiss T, Sleziak R, Stoeckli-Evans H. Synthesis, chiroptical properties, and solid-state structure determination of two new chiral dipyrrin difluoroboryl chelates. J Am Chem Soc 2004;126:1772–80.
[13] Zhao L, Wang K, Furuyama T, Jiang J, Kobayashi N. Synthesis and spectroscopic properties of chiral binaphthyl-linked subphthalocyanines. Chem Commun 2014;50:7663–5.
[14] Kobayashi N, Higashi R, Titeca BC, Lamote F, Ceulemans A. Substituent-induced circular dichroism in phthalocyanines. J Am Chem Soc 1999;121:12018–28.
[15] (a) Zhou Y, Zhu Z, Huang W, Liu W, Wu S, Liu X, et al. Optical coupling between chiral biomolecules and semiconductor nanoparticles: size-dependent circular dichroism absorption. Angew Chem Int Ed 2011;50:11456–9.
(b) Han B, Zhu Z, Li Z, Zhang W, Tang Z. Conformation modulated optical activity enhancement in chiral cysteine and Au nanorod assemblies. J Am Chem Soc 2014;136:16104–7.
(c) Zhao L, Qi D, Wang K, Wang T, Jiang J, Han B, et al. Integration of inherent and induced chirality into subphthalocyanine analogue. Sci Rep 2016;6:28026.
[16] Zhao Y, Truhlar DG. The M06 suite of density functionals for main group thermochemistry, thermochemical kinetics, noncovalent interactions, excited states, and transition elements: two new functionals and systematic testing of four M06-class functionals and 12 other functionals. Theor Chem Acc 2008;120:215–41.